X-ray Diffraction Evidence for the Existence of 102.0- and 230.0-nm Transverse Periodicities in Striated Muscle

J. Bordas,* G. R. Mant,* G. P. Diakun,‡ and C. Nave‡

*Medical Research Council/Science and Engineering Research Council Biology Support Laboratory; and
‡Science and Engineering Research Council, Daresbury Laboratory, Warrington WA44AD, Great Britain

Abstract. Synchrotron radiation techniques have enabled us to record meridional x-ray diffraction patterns from frog sartorius muscle at resolutions ranging from ~2,800 to 38 nm (i.e., overlapping with the optical microscope and the region normally accessible with low angle diffraction cameras).

These diffraction patterns represent the transform of the low resolution structure of muscle projected on the sarcomere axis and sampled by its repeat. Altering the sarcomere length results in the sampling of different parts of this transform, which induces changes in the positions and the integrated intensities of the diffraction maxima. This effect has been used to determine the transform of the mass projection on the muscle axis in a quasicontinuous fashion. The results reveal the existence of maxima arising from long-range periodicities in the structure. Determination of the zeroes in the transforms has been used to obtain phase information from which electron density maps have been calculated.

The x-ray diffraction diagrams and the resulting electron density maps show the existence of a series of mass bands, disposed transversely to the sarcomere axis and distributed at regular intervals. A set of these transverse structures is associated with thin filaments, and their 102.0-nm repeat suggests a close structural relationship with their known molecular components. A second set, spaced by ~230.0 nm, is also present; from diffraction theory one has to conclude that this repeat simultaneously exists in thick and thin filament regions.

THE sarcomere is the crystallographic, as well as the physiological, unit cell of muscle at low resolution. Upon stretching muscle fibers, the sarcomeres retain uniform registration along its length. This property provides a high degree of one-dimensional long-range order with a variable crystallographic unit cell.

The sliding filament model (11, 12) provides a structural basis for muscular contraction. In this model the sarcomere is described as consisting of thin filaments (mostly actin), emanating from the transverse Z bands (delimiting the sarcomere ends), and of thick filaments (mostly myosin) emanating from the M bands, which bisect the sarcomere. The Z and M bands are a symmetry plane for the thin and thick filaments, respectively. The thick filament region (A band) has a total length of ~1,600 nm. The length of the thin filaments (as measured from the Z band) is ~1,000 nm. In the region of overlap the thick and thin filaments interdigitate, forming a hexagonal lattice. The name I band is reserved for the portion of the thin filaments in the nonoverlap region. The sliding filament model states that muscular contraction proceeds by a change in the degree of overlap between thick and thin filaments, without any change in their length. Thus, the I band shortens, while the A band remains unchanged. Although highly successful in accounting for muscular contraction, this model does not provide an explanation for the forces that hold the sarcomere together.

A number of proteins, other than those directly involved in the contractile process, and which do not relate in any obvious way to the sliding filament model, are known to exist. Titin and nebulin (21, 22) appear to be the most abundant among them and together they comprise ~12–14% of the myofibrillar mass. Also, there is evidence for the existence of a complex network of longitudinal and transverse intermediate filaments, which have been detected after solubilization of the main proteins (8, 23). Transversely disposed mass bands, named N lines, were revealed by early electron microscopy investigations in tortoise (17) and frog muscles (7) as two pairs of bands (N1 and N2, respectively) symmetrically disposed around the Z band. More recent electron microscopy observations in unstained isolated myofibrils (5) indicate that symmetrical pairs of cross-striations in the I band, including the N lines, may form a lattice with spacings of ~230.0 nm. The term pseudolattice might be more appropriate in this context as the model described in reference 5 states that these striations have a differential length dependence when the sarcomere is stretched to lengths in excess of ~2,800.0 nm. The existence of 230.0-nm periodicities was also suggested by the positions of some of the meridional

reflections in x-ray diffraction patterns indexing as higher orders of a 229.5- (muscle at rest length and relaxed) or a 231.5-nm repeat (muscle in rigor) (9).

A great deal of current x-ray diffraction with synchrotron radiation (SR)[1] is devoted to the understanding of the molecular mechanism by which the force needed to induce muscle contraction is generated (14). However, x-ray diffraction studies of the long-range structural organization of intact, live muscle are absent in the literature. The reasons are mostly technical, as the normally used low angle x-ray diffraction cameras (3) are inadequate for this purpose. Nevertheless, the high spectral brilliance of SR sources has all the optical properties needed to resolve the closely spaced diffraction orders that a large cell like the muscle sarcomere will yield (16).

We present below x-ray diffraction evidence for the existence of a series of transverse electron density bands with long-range periodicities. These bands are not accounted for by the known structural features in the thin and thick filaments.

Materials and Methods

Determination of Transforms

The very low angle meridional reflections arise from the sampling by the sarcomere repeat of the transform of the mass projection on the muscle axis. Being able to alter the unit cell means that the transforms can be determined in a quasicontinuous fashion and that these reflections can be phased using the modification of the minimum wavelength method (4) described below.

We define the repeating unit as consisting of two regions. (*a*) The region symmetrically disposed on either side of the Z lines and consisting mainly of thin filaments (notice that this includes the whole of the thin filaments and not just the I band). (*b*) The region symmetrically disposed on either side of the M line and consisting mainly of thick filaments. The mass projections of both regions are respectively centrosymmetric around the Z and M lines; consequently, their transforms will have only zero or π as phases. The Z and M lines are separated by half the sarcomere length ($L/2$). If the transform of the first and second region are referred as $F_1(Z)$ and $F_2(Z)$, respectively, then the transform of the whole unit cell is given by: $F(Z) = F_1(Z) + F_2(Z)\, e^{\pi LZi}$ where Z is the meridional coordinate in reciprocal space. The modulus of Z is defined as $2\sin\theta/\lambda$, where θ is half the diffraction angle and λ the wavelength in nanometers (i.e., in inverse real space dimensions). The term $e^{\pi LZi}$ accounts for the phase relationship between the first and the second region.

The one-dimensional order associated with the sarcomere repeat will produce meridional reflections corresponding to the product of the meridional lattice transform (i.e., zero everywhere except at the discrete values of $Z = n/L$, for $n = 0, \pm1, \pm2$, etc . . .) with the total transform F. It is straightforward to show that if F_n is the structure amplitude of the nth order, then: $F_n = F_1(n/L) - F_2(n/L)$ for odd values of n and $F_n = F_1(n/L) + F_2(n/L)$ for even values of n.

By stretching the muscle the odd and even orders will continuously sample $F_1 - F_2$ and $F_1 + F_2$, respectively; thus, the transforms of the two components of the unit cell can be determined. Any prominent maxima present in these continuous transforms are due to repeats within the molecular components of the sarcomere or to higher orders of these repeats. Also, these functions will go through a zero whenever there is a change of phase. Hence, by determining the position of the zeroes and the sign of two reflections and by applying the sampling theorem (15), it is possible to phase the diffraction patterns and determine the mass projection on the muscle axis.

Muscles

The experiments were carried out on sartorius muscles from *Rana esculenta*. The muscles were dissected in cold Ringer's solution and either used immediately or stored for up to 5 h in a cold room before the measurements. While in storage or during the measurements the muscles were bathed in continuously oxygenated Ringer's solution. The muscles were mounted on Perspex cells equipped with thin mylar or mica windows placed very close to the specimen. The windows allowed transmission of x-rays through a region ~10 mm from the pelvic attachment. The pelvic end of the muscles was clamped to the cell. The tendon at the opposite end was attached with cotton to a stainless steel wire that was itself attached to a fine micrometer. Measurements were performed at room temperature.

Muscles were set at approximately rest length and then allowed to shorten or were stretched. The required sarcomere lengths were determined by the positions of the x-ray diffraction orders. The protocole used for any given muscle consisted of obtaining a full data set (e.g., Fig. 1) followed by the coverage of a smaller region of the diffraction pattern (typically using five or six diffraction orders) with small stretches in between the measurements (e.g., Fig. 2 *b*) or the reverse procedure. This allowed an appraisal of the consistency of the data. To obtain a complete sampling of the transforms at high resolution, the sarcomere lengths were allowed to shorten to adopt a minimum length (values of the sarcomere at ~2,050.0 nm were obtained in this way, e.g., Fig. 2 *a*, i) and then stretched by small amounts in between the recording of the patterns. Several stretches, adding up to a total of ~200 nm, are sufficient to continuously sample the transforms at resolutions >0.005 nm^{-1}. Two neighboring orders were usually allowed to pass through the same region of the transform (i.e., maximum stretches of ~400.0 nm) and the consistency of the results was checked in this way. The longest sarcomere length used in the measurements was 2,780.0 nm (Fig. 2 *a*, v). For lengths at around this value noticeable loss of sampling could be detected in the high resolution region of the diffraction patterns (e.g., Fig. 2 *a*, v).

Ultra-small Angle x-ray Diffraction Camera

The sarcomere repeat is very large in comparison to commonly studied crystallographic cells. Consequently, the diffraction maxima arising from its sampling are very closely spaced in angle. To resolve them it is necessary to record the patterns with unusually high angular resolutions. The combination of perfect crystal monochromators and SR sources provides the means to achieve the required angular resolution and retain high enough fluxes to collect statistically significant data.

The monochromator consisted of a channel cut, four reflections, Si 111 crystal. The majority of the diffraction patterns were recorded at a wavelength of 0.155 nm. Some diffraction patterns were also collected with a wavelength of 0.1488 nm. The use of these two wavelengths made no difference to the data. The absolute values of the wavelength were calibrated from the well known positions of the K edges of Cu and Ni foils. The diffraction pattern produced by the muscle was scanned with a second identical analyzer crystal. Because the analyzer crystal only allows transmission of the x-rays contained in the angular range of its rocking curve (~7 s of arc), an effect equivalent to scanning a very narrow slit through the diffraction pattern is achieved. The scans were performed with an accuracy of 0.2 s of arc. Design details of this prototype ultra-small angle x-ray diffraction camera are described elsewhere (16). The only difference between this camera and that described in reference 16 is that the specimens were placed at the center of rotation of the analyzer crystal. With this modification the instrument can operate with short crystals while the beam cross section seen by the analyzer remains constant throughout the range of scattering angles. The diffracted photons, transmitted through the analyzer crystal, were detected with an energy-dispersive Ge solid-state detector. The solid-state detector enabled the rejection of any parasitic wavelength that might have been allowed through by the optics.

The experiments were done using the SR source at Daresbury Laboratory. The SR source was running at 2 GeV energy and mean currents of 150 mA. Under these conditions the camera provides a mean flux of 5×10^8 photons/s with a beam cross section of 2×10 mm^2. The camera was placed at ~28 m from the source. This distance was dictated by the position of the hutch in the available test station. The flux could be increased by at least a factor of five by installing the camera closer to the tangent point. For a source with the characteristics of the SR source this would not entail a significant deterioration in the angular resolution.

As it was set up, it took ~4.5 h to collect a complete set from ~2,800.0–38.0-nm resolution, with 2 s data collection per point.

Data Collection and Data Reduction

Radiation damage effects were checked by repeating scans over the same region of the diffraction patterns and the onset of damage was judged by the deterioration of the strength of a given diffraction maximum. Radiation damage could be seen after ~7-h exposure. This tolerance to radiation dam-

1. *Abbreviation used in this paper*: SR, synchrotron radiation.

age agrees well with previous experience on exposure of biological material to similar wavelengths (2). The tolerance to irradiation decreased dramatically when 0.05-nm wavelengths were tried. This suggests that the increased ionizing power of the radiation more than compensates for the much lower absorption of the specimen.

The modulus of the meridional reciprocal coordinate (Z) was calibrated from the absolute wavelength measurements and the angle of diffraction.

The diffraction maxima are superimposed on a diffuse background, which, except in the region of the first few orders, arises from the muscle itself (Fig. 1 *a*). Multiplication of the diffraction patterns by the square of their corresponding Z-axis compensates for the decay of intensities with increasing angles (Fig. 1 *b*) and simplifies the procedure of fitting a spline function through the best defined minima in the patterns. This function is then subtracted from the data. The resulting diagrams (Fig. 1 *c*), corresponding to the diffraction maxima weighted by the Z^2 correction, were separated into individual files containing only one diffraction maxima at a time. Whenever diffraction maxima overlaped significantly (e.g., in the region around 0.0098 nm^{-1}), peak stripping techniques were used. The resulting files were then divided by the square of the corresponding Z-axis (i.e., the Z^2 weighting is removed) and the integrated intensities were calculated to obtain the corresponding structure factors. We found that this procedure yields better results than simply fitting a function on the background of the unweighted diffraction diagrams. This is because fitting a background function (whether a polynomial or a cubic spline) over an intensity range of more than two and a half orders of magnitude leads to instabilities in the fitting that affect the reproducibility of the integrated intensities. The moduli of the structure amplitudes were obtained by taking the square root of the structure factors.

All the patterns were normalized for variations in the impinging flux due to the decay of the stored current in the SR source. This normalization was achieved by placing an ion chamber after the specimen and continuously monitoring the flux falling on it. A further normalization to account for variations in the diffraction volumes is also needed. This correction was done by scaling the patterns from different muscles (or for the same muscle at different lengths) using the diffraction maxima occurring at the same spacing. In any given muscle the latter correction was always small (never exceeding 15%).

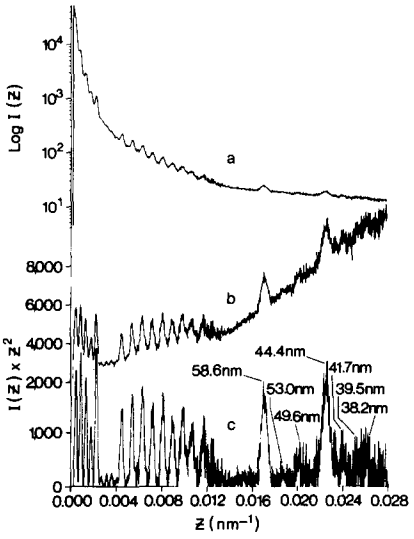

Figure 1. Illustration of a typical x-ray diffraction pattern from frog sartorius muscle at very low angles. (*a*) Logarithm of the meridional diffraction pattern from frog sartorius muscle at a sarcomere length of 2225.0 nm. (*b*) Linear display of the data in *a* after multiplication of the diffracted intensities by the square of the Z-axis. (*c*) Diffraction pattern (multiplied by the square of the Z-axis) after removal of the diffuse background. The diffraction maxima up to 0.014 nm^{-1} are orders of the sarcomere repeat (see text). Beyond 0.014 nm^{-1} a number of reflections that do not index with the sarcomere repeat can be seen. The reflection at 0.017 nm^{-1} (58.6-nm spacing) was only prominent in some muscles. The reflections at ~0.0188, 0.0201, 0.022675, 0.02398, 0.0253, and 0.0261 nm^{-1} agree in spacings (~53.3, 49.6, 44.1, 41.7, 39.5, and 38.2 nm, respectively) with previous reports (9, 13). We did not investigate the dependence of these reflections on the sarcomere length.

Results

A typical result is shown in Fig. 1. Some of the features in this pattern are observed at all sarcomere lengths. A group of reflections, indexing as odd and even orders of the sarcomere repeat, are always seen at low values of Z. Beyond this region ($Z > 0.0055$ nm^{-1}), with the one exception described below, only the even orders are detectable. Even order reflections are observed to resolutions of ~70 nm ($Z < 0.014$ nm^{-1}) and then they disappear rather abruptly. The diffraction maxima show a progressive broadening with increasing order number.

The sharp definition of the low orders testifies for a very long coherent length in the structure. The progressive increase in width can be best explained by a distribution of values around the mean sarcomere repeat. A spread with a halfwidth of 5–10% around the mean can be estimated.

The diffraction orders undergo prominent changes in position and intensity as a function of the sarcomere length. Fig. 2 *a* provides an illustration.

An exception to the absence of the odd orders occurs at

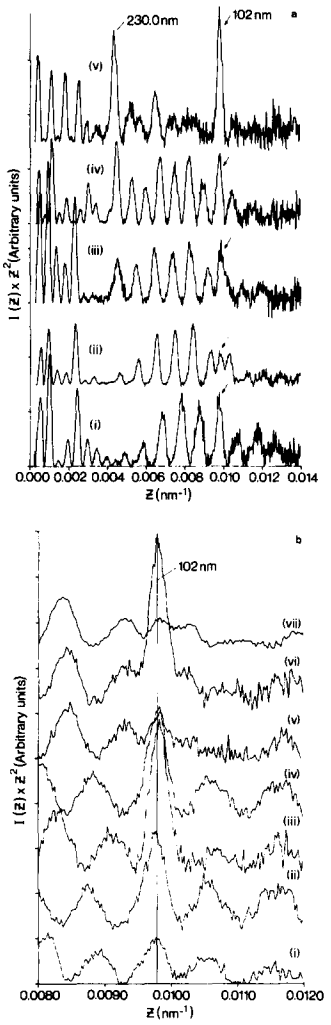

Figure 2. Very low angle diffraction patterns of frog sartorius muscle over a range of sarcomere lengths. (*a*) Diffraction patterns at ~2,044.0-, 2,140.0-, 2,170.0-, 2,667.0- and 2,780.0-nm sarcomere lengths (*i–v*, respectively). Notice the loss of sampling in *v*. The maximum at a spacing of 230.0 nm (0.00433 nm^{-1}) may be partly or totally sampled. Notice that in *ii* an odd order is seen in the neighborhood of 0.0098 nm^{-1} and that a stretch of only 30.0 nm (*iii*) is sufficient to alter its intensity while its position hardly changes. A combination of incomplete sampling and a pronounced maximum in the meridional projection of the molecular transform is responsible for this effect (see text). (*b*) Selection of patterns illustrating how the prominence of diffraction maxima at 102.0-nm spacings (0.0098 nm^{-1}) critically depends on small changes in the sarcomere lengths. Notice how the prominence of the 102.0-nm maxima increases with very small stretches. Notice also that it reaches the same maximum strength for odd (*vi*) and even (*iii*) orders. This behavior is due to a 102.0-nm repeat in the meridional mass projection of one of the components of the unit cell (see text).

0.0098 nm^{-1} (i.e., 102.0 nm spacing). A diffraction maximum is always present in this region. Its strength depends very critically on the sarcomere length. Whenever the sarcomere is adjusted to a multiple of this spacing, the strength of this maximum increases severalfold. This happens irrepectively of whether this spacing is an odd or an even submultiple of the sarcomere length. The development of this maximum with fine adjustments of the sarcomere length is shown in Fig. 2 *b*. The highest intensities reached are the same for the odd and the even orders.

Whenever the sarcomere is stretched by 20–25% above its rest length some of the orders tend to dissappear or merge with each other. The reflection at 102.0 nm spacing remains. Another diffraction maximum at ~230.0 nm spacing shows prominently. The simplest explanation for these observations (Fig. 2 *a*, v) is that one is detecting structural disruption in the register of the sarcomeres. However, the internal structures from which these periodicities arise are somehow preserved. Notice that length increases of the order of 20% coincide with the onset of significant passive tension (10). The reflections at spacings of 102.0 and ~230.0 nm remain strong, indicating they are maxima in the transform and reflect the spacing between structures within the sarcomere.

Fig. 3 *a* shows that the continuous transform of $F_1(Z) - F_2(Z)$ becomes negligeably small beyond 0.0055 nm^{-1} (except in the neighborhood of 102.0-nm spacings). Fig. 3 *b* illustrates that the continuous transform of $F_1(Z) + F_2(Z)$ has two particularly well defined maxima at spacings of ~230.0 and 102.0 nm. The centroid of the former corresponds to spacings between 229.0 and 230.0 nm or at a spacing of 231.2 if judged by the position of the strong reflection in Fig. 2 *a*, v. The spacing of the latter can be determined much more accurately and corresponds to 102.0 ± 0.02 nm.

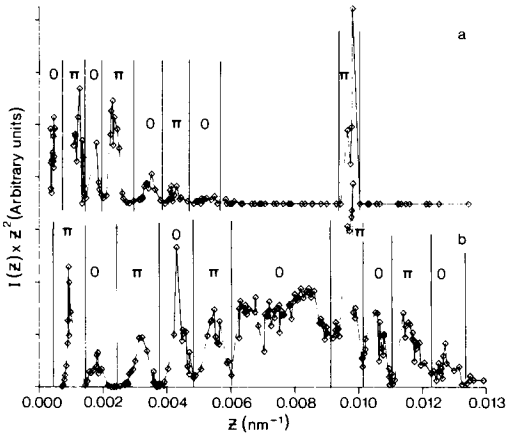

Figure 3. Illustration of the dependence of the integrated intensities of the odd and even orders on the sarcomere length. The integrated intensities for the odd and even orders were obtained from a total of 16 muscles. For illustration purposes the integrated intensities are displayed after multiplication by the square of their corresponding Z vector. The continuity of the transform for $Z < 0.0015$ nm^{-1} cannot be followed because the muscles would have to be stretched to sarcomere lengths in excess of 6,000.0 nm. (*a*) Continuous transform corresponding to $F_1(Z) - F_2(Z)$ (see text). This transform has been reconstituted from the integrated intensities of the odd orders. With the exception of the pronounced maximum centered at ~0.0098 nm^{-1} the integrated intensities for the odd orders can only be obtained for $Z < 0.0055$ nm^{-1}. Beyond this region they are too weak to measure. The integrated intensities obtained from the first orders ($Z < 0.0005$ nm^{-1}) have large errors, particularly for the longer sarcomere lengths, due to their lying on the rapidly sloping background from the tails of the rocking curve. (*b*) Continuous transform corresponding to $F_1(Z) + F_2(Z)$ (see text). This transform has been reconstituted from the integrated intensities of the even orders. Their integrated intensities can be measured up to 0.014 nm^{-1}. The phases used in the calculation of electron density maps are displayed in between the vertical bars. The position of the bars indicates where we judged the phase change sign (see text).

The absence of the odd orders at higher angles can be explained by recalling the considerations in Materials and Methods. As the odd orders sample the difference of the transforms of the two components of the unit cell, their absence must be due to a set of electron density maxima in the axial mass projection, common to both components, and dominating the diffraction patterns in this region. The 230.0-nm maximum is absent in the quasicontinuous transforms deduced from the odd orders, while it is particularly sharp and prominent in that deduced from the even orders. This indicates that this repeat is common to both components of the unit cell. The maximum at a spacing of 102.0-nm appears in odd and even orders; consequently, this periodicity must exist in the sum and in the difference of the transforms. Because the highest intensities reached by this maximum are the same, within error, for odd and even orders, the implication is that this spacing exists in only one of the components of the unit cell.

A value of 102.0 nm coincides with a near exact multiple of the spacing of the 5.097-nm layer line arising from the one-start helix in the actin filament (13). Thus, the thin filament region is the likely candidate for this repeat.

The observations on the 230.0-nm repeat agree with recent electron microscopy data and support the model proposed in reference 5. We have found no evidence in the literature for the repeat with 102.0-nm spacings that our data demonstrates.

Electron Density Maps

The transforms shown in Fig. 3 can be used for phase assignment if the zeroes can be unambiguously established.

In an ideal case, a phase reversal would be characterized by a value of zero in the structure factor at the corresponding spacing. Minima would only indicate dips in the transform but without an associated phase change. In our case the spread in the sarcomere length and, possibly, other disorder effects imply the sampling of an extended portion of the transform; hence, some of the observed minima, even if they do not reach a value of zero, may also be due to a phase reversal.

Simple models of the sarcomere can be used to determine the phases for $Z < 0.002$ nm^{-1}. The well known fact that there is less mass in the I than in the A band is sufficient to determine the phases in this region. The signs were also checked by calculating the amplitudes and phases yielded by a number of simple models built from estimates of the relative densities of the various protein components in muscle (e.g., Fig. 4).

The phases in the region of $0.002 < Z < 0.0055$ nm^{-1} were obtained by sign reversal after each minimum in Fig. 3.

The diffraction maxima between 0.006 and 0.009 nm^{-1} do not reach a small enough value to warrant the presence of a

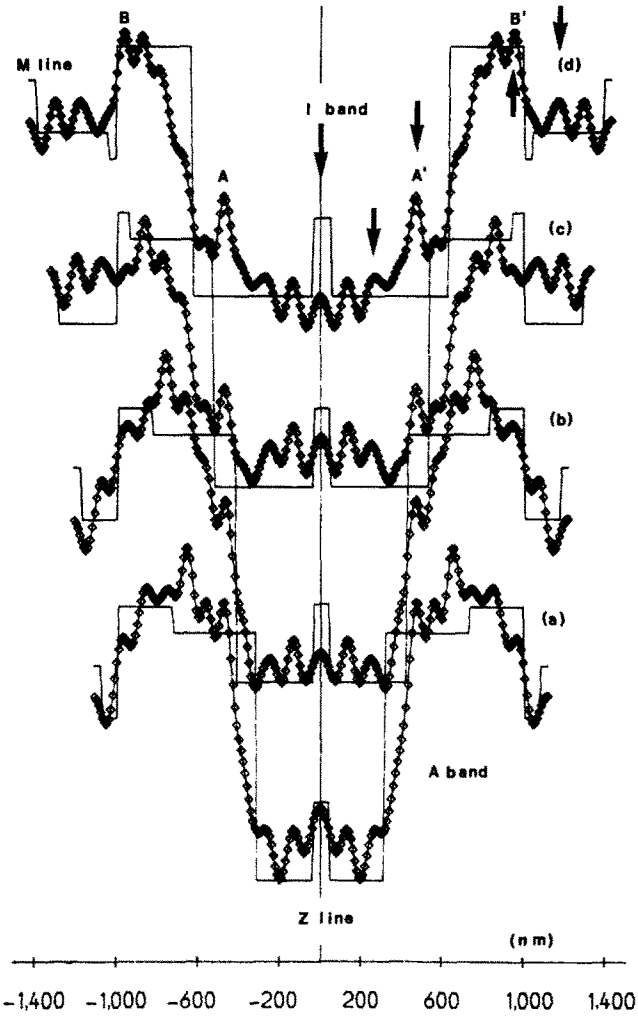

Figure 4. Calculated electron density projections on the meridian of the muscle fiber (line of diamonds). These maps are calculated from the data shown in Fig. 3. They correspond to sarcomere lengths of 2,235.0, 2,438.0, 2,641.0, and 2,848.0 nm (*a–d*). The maps are displayed aligned at the Z line. The maps show a number of common features associated with thick and thin filaments. As the sarcomere length increases the overlap changes and the I band broadens, also some of the features can be more clearly seen. The continuous lines correspond to the mass projection of simplified models in which the myosin, actin, M line, Z lines, and C protein are included.

zero. This is expected as in this resolution range one is mostly sensitive to features common to both components of the unit cell (i.e., absence of odd orders), hence the phases must also be identical. One-dimensional electron density maps calculated with a phase of π in this region invariably lead to the absence of the Z and M lines. This is an unlikely solution. We concluded that the phase must be zero, in which case the minimum at 0.006 nm^{-1} (see Fig. 3 *b*) must be due to a phase reversal.

Another uncertainty arises between 0.009 and 0.011 nm^{-1}. The intensities of the even orders decrease to a minimum at ~0.0093 nm^{-1}. This is followed by a rise to a peak at 0.0098 nm^{-1} and then a drop to another minimum at 0.0101 nm^{-1} (see Figs. 2 *b* and 3 *b*). This suggests the presence of two potential zeroes. Nevertheless, due to the partial sampling and overlap in this region, these two minima, in particular the first one, are not well defined. It is difficult to decide whether they are due to genuine zeroes or not. To resolve this ambiguity we calculated electron density maps with both possible types of phases for a number of sarcomere lengths. We decided that π probably is the best choice. This is based on the criterion that features associated with either thin or thick filaments clearly persist over a range of sarcomere lengths and also on the basis that this phase places the contribution of the 102.0-nm spacing in the thin filament region. If a phase of zero is assigned to this maximum, the main effect on the electron density maps would be to place the 102.0-nm periodicity in register with the Z-band, rather than out of register by half a repeat (see Discussion).

The best set of phases we obtained with these procedures are shown in Fig. 3 *a* and *b*. The vertical lines delimit the regions in which we judged a change of phase takes place.

Once the continuous transform and the associated phases are determined, it is straightforward to calculate the one-dimensional electron density maps representing the meridional mass projections for any sarcomere length. This enables the separation of the density in the thin and thick filaments and reveals which maxima are associated with them. Because of the procedure used to determine the transforms at high resolution, the electron density maps at long sarcomere lengths would correspond to those expected if the internal structure of the two components of the unit cell remained unchanged after stretching (see Discussion).

Fig. 4 shows a selection of these maps. The maps at shorter sarcomere lengths (Fig. 4, *a* and *b*) are very reminiscent of early electron microscopy observations in whole myofibrils (1).

The maps show a number of bands pairing symmetrically around the M and Z lines. Their prominence is rather variable. As the sarcomere length increases some of these bands remain associated with the thick filaments, others with the thin ones.

The bands associated with the thick filaments are placed at ~120.0, 235.0, and 465.0 nm away from the center of the M line. A fourth band, which also appears to be associated with the thick filaments, is at a distance of ~558.0 nm. These distances correlate with the positions of the strong P3, C3, C21, and D6 stripes (20) seen in electron micrographs of human *m. tibialis* anterior muscle. The C3 and C21 stripes are close to the ends of the C protein region.

Two of the pairs of bands are particularly prominent (A–A′ and B–B′ in Fig. 4); the separation between the bands in each pair is ~930.0 nm. These pairs are symmetrically placed about the Z and M lines, respectively. As the sarcomere length changes the A–A′ pair stays associated with the thin filaments, while the B–B′ pair moves with the thick ones. The separation between the bands in each pair remains constant with increasing sarcomere lengths.

Discussion

The mass projections on the muscle axis (Fig. 4) show the A and I bands expected from the overlap of the thin and thick filaments; they also display a number of other bands.

The resolution of the maps is limited to ~75.0 nm (as defined by the spacing of the highest diffraction order used in their calculation). Their limited resolution implies that

features separated by <75.0 nm will show as a single maximum; hence, their centroid will not necessarily coincide, within the resolution limits, with the position expected from any of the detected periodicities, the values of which can be extracted much more accurately from the diffraction patterns. Also, the peak to valley ratios may be artificially reduced as a result of mass being spread out over a larger region than occupied in reality. This, together with mass translocations due to stretching in the muscle (discussed below) and genuine disorder effects, implies that the maps should be taken with some caution and considered more as approximate models than a quantitative representation of the structure of the sarcomere. An unambiguous interpretation of the maps is not possible at this stage, although certain correlations with previously described features in the structure of muscle can be established.

It is important to point out that the reliability of the maps depends on the validity of the central assumption that the internal structure of the two components of the unit cell remains unaltered after stretching of the muscle. Electron microscopy observations (7, 17) showed that the N_2 lines only remained at a constant distance relative to the Z bands for sarcomeres at either below or just above rest length (~2,300.0 nm). For longer stretches, the N_2 lines moved linearly with sarcomere lengths but not in such a way that their positions relative to either the M or Z lines remained constant. This behavior would lead to errors in the electron density maps at longer lengths (Fig. 4). An estimate of these errors can be made by considering that at a sarcomere length of 2,300.0 nm, the mean separation between the Z and N_2 bands was estimated to be 215.0 nm. At a sarcomere length of 2,800.0 nm the mean distance was 320.0 nm. Scatter in the values of up to 50 nm was observed from preparation to preparation (7). Possibly because the measurements were taken in muscles from different species, the values reported in reference 17 differ by >100.0 nm from those reported in reference 7 (experiments done on turtle and frog muscle, respectively). Assuming that the separation between the N_2 and the Z bands changes linearly with the sarcomere length (7, 17), one can conclude that, for stretches ranging from rest up to 2,800.0-nm sarcomere lengths, translocation effects of this type would only have a significant effect on the intensity distribution of the diffraction orders at ~0.009 nm^{-1}. Notice that effects of this type would tend to blur the zeroes; this is possibly another reason why the minima in the continuous transforms are poorly defined in this region (Fig. 3).

The largest stretches applied in our study correspond to a sarcomere length of 2,780.0 nm (Fig. 2 *a*, v), where the onset of significant disorder in the structure can be seen. For this reason, at any given resolution, we determined the transforms with the smallest possible stretches (see Materials and Methods). The reason for this procedure is that the higher the resolution at which the transforms are sampled, the smaller are the stretches required to do it, hence, the less susceptible one is to the onset of translocation effects leading to deregister in the internal structure of the two components of the unit cell. The implication of this procedure is that the determination of the zeroes for the high resolution part of the transforms (i.e., where one is most sensitive to the internal structure) may only be correct for the shorter sarcomere lengths. In fact, we never measured at the sarcomere length corresponding to the electron density map shown in Fig. 4 *d* and this map must be seen as representing how the mass distribution within the sarcomere would look if no change in the internal structure occurred and is meant to illustrate the mass in the thin and thick filaments without the large overlap which occurs at shorter lengths. The figure also serves to reveal that the A–A′ bands are associated with the thin filaments.

More recent electron microscopy observations (5) on semitendinosus muscle appear to show that symmetrical pairs of cross-striations in the I band, including the N lines, are only shifted out of register relative to either the M or Z lines for sarcomere lengths >2,800–3,200 nm. If this was our case, then the positions of the bands in our maps would be an accurate representation of the mass density even at the longest sarcomere length. The diffraction patterns up to sarcomere lengths of ~2,700 nm are well behaved in the sense that the minima in the transforms are reproducible over the range of stretches and, also, in that no loss of sampling is detected. These observations argue in favor of the transverse bands remaining in register within the resolution of the measurements, until lengths coinciding with the onset of passive tension are reached, and suggest that, for the range of stretches used in the determination of the transforms, the calculated electron density maps, especially at the shorter lengths (Fig. 4 *a–c*) may not be unduly distorted by translocational effects. We attribute the second pair of lines disposed at ~230.0 nm on either side of the Z bands to the N_2 lines and we stress the possibility that for the longer sarcomere lengths they may be misplaced.

Electron micrographs of ferritin-labeled fibers from frog sartorius (7) showed that the N_1 lines are symmetrically placed at a mean distance of ~ 140.0 nm from the center of the Z band (a variation in the distances, ranging from 110 to 170 nm, was observed). For moderate stetches (up to sarcomere lengths of ~2,500.0 nm) the position of the N_1 band was roughly constant. The first pair of maxima on either side of the Z band in the electron density maps (at a distance of ~130.0 nm) correlate well with this observation and we interpret them as representing the position of the N_1 bands.

The mass projections in the region of the Z bands are much weaker than expected. One possible explanation could be the effect of muscle disorder in the diffraction patterns. However, it is hard to imagine that disorder would favor the suppression of the Z bands while enhancing the other bands. Another explanation may be that the diffraction patterns are sensitive to quantized deregistry in neighboring myofibrils (e.g., vernier-like shifts of 230.0 nm as described in reference 5), in which case the lines in the electron density maps would be enhanced or suppressed according to the three-dimensional organization of the myofibrils.

Given all these uncertainties, further interpretation of the electron density maps is probably impossible at this stage. However, from the x-ray diffraction patterns and their phase assignment, one can assess how the 230.0- and the 102.0-nm periodicities contribute to the electron density and correlate with recent reports (5, 24).

Diffraction theory of centrosymmetric structures shows that assignment of a zero phase to a given diffraction maxima leads to addition of mass at the ends and at the center of the unit cell. Thus, the phase assignment of zero to the transform maximum at spacings of ~230.0 nm (see Fig. 3) implies that the diffraction bands in this region will add mass in register

with the Z and M bands, with other orders modulating the strength of their contribution throughout the unit cell in accordance with their intensities and phases. This places the main contribution of the 230.0-nm periodicity to the electron density maps in the two pairs of maxima (possibly three) in the I band (including the N_2 and the A–A′ lines) and the two pairs in the A band (marked with arrows in Fig. 4). As the sarcomere length is increased the two pairs associated with the A band retain their distance relative to the M band, while the other two pairs behave identically with respect to the Z band. This differential length dependency implies that a true 230.0-nm repeat will only exist at a sarcomere length of 2,300.0 nm (i.e., at rest length), where all these bands, together with the M and Z bands, are in exact register. This differential length dependency is very much in line with the electron microscopy observations described in reference 5. A major difference, however, is that electron microscopy places the regions of enhanced contrast out of register with respect to the Z and M bands by half a 230.0-nm repeat. This discrepancy could be reconciled by making the assumption that our phase assignment to the 230.0-nm band is off by π, as then the side bands would be in antiregister with the Z and M lines (the electron density maxima would be upside down relative to those displayed in Fig. 4). One would also observe a split in the Z and M bands (although unlikely, this would not be an impossible solution if the diffraction patterns were sensitive to quantized disregistry of the myofibrils). However, the zero at 0.0038 nm^{-1} is particularly well defined (see Fig. 3) and in a region where disorder and translocation effects should have a minimal influence, which argues against this explanation. Another possibility is that the distribution of the stain used for visualization in the electron microscope enhances the contrast at grooves between mass maxima. Alternatively, there might be a genuine difference in the transverse distribution of mass in the sartorius and the semitendinosus muscle used in (5). Preliminary x-ray diffraction patterns from semitendinosus muscle show a number of discrepancies with the results we report here. The differences pertain not only to the intensity distribution in the diffraction maxima but also to the fact that the 102.0-nm band is either very weak or absent. Because of this observation and the well known differences in mechanical behavior between these two types of muscle, this latter explanation must be considered as a possibility.

Compared with the 230.0-nm repeat, the contribution of the 102.0-nm periodicity to the electron density maps is rather weak (this can be directly seen by comparing the intensity under the respective bands in Fig. 3 *b* and correcting for the Z^2 factor used for display purposes). Because of its weakness and the resolution limitations described above, this periodicity can just barely be discerned on the electron density maps. With the phase assignment of π, these repeats contribute as pairs of electron density maxima in antiregister with the Z bands. In this situation the maxima due to the 230.0- and the 102.0-nm repeats will come into register at the position of the A–A′ pairs. It may be significant that it is approximately at this position where titin and nebulin are simultaneously detected by dual immunofluorescence localization (24). In fact, within the resolution of the respective measurements, there is a good correlation between the various mass bands derived from the x-ray diffraction patterns and the placing of titin and nebulin (Fig. 13 in reference 24).

The fact that there is a common multiplicity between the 102.0- and the 230.0-nm repeats suggests a close structural relationship between these two sets of bands, although, considering that the diffraction patterns show that the 102.0-nm periodicity is present in only one component of the unit cell, while the 230.0-nm repeat exists in both, it is unlikely that they arise from a common structure with a long-range periodicity.

The most direct (and compelling) evidence for the existence of these periodicities are the diffraction patterns themselves. Irrespective of any errors in the electron density maps, the existence of these mass bands can be deduced directly from the data. The 230.0-nm periodicity has been interpreted as arising from a cytoskeletal element within the sarcomere which is simultaneously present in the A and I bands (5). The fact that this repeat is very near the 16th and the 84th multiples of the 14.3- and 2.7-nm meridional reflections (13) (representing the axial rise of the myosin heads in thick filaments and the actin molecule in thin filaments, respectively) has been used to argue a putative role for this cytoskeletal lattice as regulating the axial register of thin and thick filaments and integrating the organization of the contractile proteins within the sarcomere (5). Our data supports the existence of such a lattice. The new 102.0-nm periodicity revealed by our data suggests that the structural organization in frog sartorius muscle may be more complicated than that proposed in reference 5.

The diffraction patterns show that the 102.0 $\pm$ 0.2-nm spacing is associated with only one of the unit cell components. The close agreement of this spacing with the 20th multiple of the 5.097 $\pm$ 0.002-nm pitch of the actin helix (13) supports the assignment of this repeat to the thin filament region.

None of the conceivable structures for the actin filament would provide a meridional reflection at 102.0-nm spacing. Consequently, it must originate from some actin-associated protein. The reflection is confined to the meridian, implying that this actin-associated protein may span across the sarcomere or that it may have a superhelical organization bearing a close relationship to the thin filaments, the axial rise of which would yield the 102.0-nm reflection, or both.

The fact that the 5.097-nm layer lines index as a submultiple of a long-range repeat in the spatial disposition of some actin-associated protein implies that the actin helix itself might also have it. However, a repeat in the actin helix at every 102.0 nm is not compatible with the very accurate measurements of the positions of the other actin diffraction maxima (13). It can be shown from helical diffraction theory that the lowest helical repeat, compatible with the known periodicities of the actin filament (within the errors reported in reference 13) and which is also a multiple of 102.0 nm, corresponds to six times 101.94 nm (i.e., 611.64 nm). This helix would have 22.3/12 subunits per turn of the 5.097-nm pitch helix (or just over 2.165 subunits per turn of the genetic helix, i.e., a slightly underwound version of the often used approximation of 28/13 subunits per turn of the genetic helix). The spacings of the layer lines indexing with Bessel functions of fourth order or less (i.e., low enough Bessel function order to be expected experimentally) are, within error, in agreement with the observations up to a resolution of 2.7 nm (9, 13). Two layer lines at spacings of 35.97 and 17.98 nm are predicted (J_2 and J_4 Bessel functions, respectively). These layer lines are not clearly observed in the x-ray diffraction

diagrams from this muscle at rest. Their lack of prominence has been attributed to cumulative azimuthal angular disorder in the actin helix (6). During contraction an actin-associated layer line at a spacing of 17.93 ± 0.15 nm develops (14). The intensity in this layer line increases at a radial distance expected for a J_4 Bessel function. This layer line is also compatible with this long-range repeat in the actin structure. Actin-associated reflections extend to very high resolution in frog sartorius muscle (13). All of the reported higher order spacings index as submultiples of this long repeat; however, it is not possible to assign compatible Bessel functions to the reflections at spacings of 2.04, 1.106, and 0.785 nm or the meridional reflection at ~5.9-nm spacing (13). In this model, these reflections would be forbidden by helical symmetry and arise from the long repeat of the actin-associated lattice.

The spatial relationships described above indicate that an actin helix with a long-range repeat, held in place by a lattice of actin-associated proteins, should be considered as a possible feature of the structural organization of thin filaments. The existence of such a lattice is supported by the presence of the 102.0-nm periodicity and the implied actin long-range repeat is compatible with the x-ray evidence at higher angles. This possibility (unproven so far) has to be considered against subtler ways whereby the thin filament region could display axial repeats every 102.0 nm. For instance, one can contemplate an arrangement in which various coexisting structural elements have repeats that come into register at common multiples. One of the meridional reflections, forbidden by helical symmetry, occurs at a spacing of 38.6–38.8 nm (13). This reflection is believed to originate from the repeat of the tropomyosin–troponin complex along the actin filament (18). This reflection is in fact split into two maxima at spacings of 39.5 and 38.2 nm (9, 13). These two maxima have similar intensities (see Fig. 1). A feature of the structure of striated muscle is that, from a diffraction point of view, it behaves like a set of gratings with variable center to center distances. The consequence of this arrangement is that any prominent periodicities are expected to be accompanied by subsidiary maxima due to the interference set up with their corresponding mirror image on the opposite side of the Z or the M bands (19). Interference effects of this type have been used to explain the splitting of the 38.5-nm reflection. Nevertheless, the 16th submultiple of the 611.64 repeat happens to coincide with the position of the 38.2-nm spacing and suggests yet another structural relationship between this repeat and the positioning of the tropomyosin–troponin complex in thin filaments.

The spatial relationships between the 102.0-nm repeat and the well known thin filament periodicities, together with those previously described for the 230.0-nm repeat (5), amount to a significant body of evidence, outside that expected from a random set of coincidences, in favor of the view that within the sarcomere there is a set of structures coordinating the mutual disposition of thick and thin filaments. While the full significance of these relationships and of the role of these putative lattices is difficult to ascertain, the results suggest that some of the proteins forming the complex network of longitudinal and transverse filaments (8, 23) may be distributed at regular intervals, with repeats that are multiples of the known periodicities in thin and thick filaments. Given the relative abundance of titin and nebulin (24), it is not unreasonable to assume that these proteins may be involved in the formation of these structures.

Received for publication 30 September 1986, and in revised form 19 February 1987.

References

1. Bennett, H. S., and K. R. Porter. 1953. An electron microscope study of sectioned breast muscle of the domestic fowl. *Am. J. Anat.* 93:61–105.
2. Bordas, J., and E. M. Mandelkow. 1983. Time resolved X-ray scattering from solutions using synchrotron radiation. *In* Fast Methods in Physical Biochemistry and Cell Biology. R. I. Sha'afi, and S. M. Fernandez, editors. Elsevier/North Holland Biochemical Press. Amsterdam: 137–172.
3. Bordas, J., 1985. Synchrotron radiation X-ray scattering and diffraction: applications to structural research in biology. *Z. Phys. B. (Condensed Matter).* 61:389–395.
4. Bragg, W. L., and Perutz. 1952. The structure of haemoglobin. *Proc. R. Soc. Edinb. Sect. A (Math. Phys. Sci.).* A213:425–435.
5. Cooke, P. 1985. A periodic cytoskeletal lattice in striated muscle. *Cell Muscle Motil.* 6:287–313.
6. Egelman, H. E., N. Francis, and D. J. DeRosier. F-actin is a helix with a random variable twist. *Nature (Lond.).* 298:131–135.
7. Franzini-Armstrong, C. 1970. Details of the I band structure as revealed by the localization of ferritin. *Tissue & Cell.* 2:327–338.
8. Granger, B. L., and E. Lazarides. 1978. The existence of an insoluble Z disc scaffold in chicken skeletal muscle. *Cell.* 15:1253–1268.
9. Haselgrove, J. C. 1975. X-ray evidence for conformational changes in the myosin filaments of vertebrate striated muscle. *J. Mol. Biol.* 92:113–143.
10. Hill, A. V. 1950. Mechanics of the contractile element of muscle. *Nature (Lond.).* 166:415–419.
11. Huxley, A., and R. Niedergerke. 1954. Structural changes in muscle during contraction. *Nature (Lond.).* 173:971–973.
12. Huxley, H., and J. Hanson. 1954. Changes in the cross-striations of muscle during contraction and stretch and their structural interpretation. *Nature (Lond.).* 173:973–976.
13. Huxley, H. E., and W. Brown. 1967. The low angle X-ray diagram of vertebrate striated muscle and its behavior during contraction and rigor. *J. Mol. Biol.* 30:383–434.
14. Kress, M., H. E. Huxley, A. R. Faruqi, and J. Hendrix. 1986. Structural changes during activation of frog muscle studied by time-resolved X-ray diffraction. *J. Mol. Biol.* 188:325–342.
15. Makowski, L. 1981. The use of continuous diffraction data as a phase constraint. I. One dimensional theory. *J. Appl. Crystallogr.* 14:160–168.
16. Nave, C., G. P. Diakun, and J. Bordas. 1986. Ultra small angle X-ray diffraction from muscle. *Nucl. Instr. Methods.* A246:609–612.
17. Page, S. G. 1968. Fine structure of tortoise skeletal muscle. *J. Physiol. (Lond.).* 197:709–715.
18. Rome, E., T. Hirabayashi, and S. V. Perry. 1973. X-ray diffraction of muscle labeled with antibody to troponin C. *Nature (Lond.).* 244:154–155.
19. Rome, E. 1973. Structural studies by X-ray diffraction of striated muscle permeated with certain ions and proteins. *Cold Spring Harbor Symp. Quant. Biol.* 37:331–339.
20. Sjostrom, M., and J. M. Squire. 1977. The structure of the A band of human skeletal muscle fibres from ultra thin negatively stained cryosections. *J. Mol. Biol.* 109:49–68.
21. Trinick, J., P. Knight, and A. Whiting. 1984. Purification and properties of native titin. *J. Mol. Biol.* 180:331–356.
22. Wang, K. 1982. Purification of titin and nebulin. *Methods Enzymol.* 264–273.
23. Wang, K., and R. Ramirez-Mitchel. 1983. A network of tranverse and longitudinal intermediate filaments is associated with sarcomeres of adult vertebrate skeletal muscle. *J. Cell Biol.* 96:562–570.
24. Wang, K. 1985. Sarcomere-associated cytoskeletal lattices in striated muscle: review and hypothesis. *Cell Muscle Motil.* 6:315–369.